J. Fluid Mech. (1966), *vol.* 24, *part* 1, *pp.* 41–63
Printed in Great Britain

Computation and measurement of Hall potentials and flow-field perturbations in magnetogasdynamic flow of an axisymmetric free jet

By DAVID R. OTIS†
University of California, Berkeley

(Received 1 February 1965)

The interaction was observed between a supersonic free jet of partially ionized argon and the magnetic field of a coil concentric with the jet. Nominal values of the parameters were: Mach number, 3; Reynolds number, 1000; magnetic Reynolds number, 0·2; magnetic interaction parameter, 1; Hall parameter, 1. The jet was strongly channelled. Axial and radial electric fields were observed in the jet with a net rise in potential across the interaction.

These observations were consistent with predictions based on the single fluid, macroscopic equations, and a simple slug flow model. The current equation was solved to second order in the Hall parameter giving a closed form expression for the Hall potential which agreed with the experiments for weak fields. Flow perturbations were calculated for Mach numbers of 3.11, 6.08, and 10.05, neglecting Hall currents; the calculations are in qualitative agreement with the experiments and show Joule heating to be the main factor in perturbing the flow at high Mach numbers.

1. Introduction

Some exploratory experiments in an arc-heated wind tunnel showed a strong interaction between the gas flow and magnetic fields having various geometries and nominal values of 1000 G. There appeared a variety of phenomena which was not understood at that time, and this study was an attempt to shed light on the simplest magnetic-field configuration tested: that of gas flowing along the axis of a Helmholtz coil.

The meanings of symbols used in the paper are defined in the following list.

Notation

a = jet radius
b = plasma radius
$\mathbf{B}$ = magnetic-field vector
c_p = specific heat
$\mathbf{e}_r, \mathbf{e}_\theta, \mathbf{e}_z$ = unit vectors
$\mathbf{E}$ = electric field vector
$\mathbf{F}_n$ = Lorentz force due to nth-order current
$\mathbf{j}$ = electic-current vector
K = Hall parameter, see equation (3.14)
L = characteristic length
M = Mach number, see equation (3.11)
n_i = ion number density
p = pressure

† Present address: Mechanical Engineering Department, University of Wisconsin, Madison, Wisconsin.

p_i = impact pressure
q = charge density
R = gas constant
R_M = magnetic Reynolds number, see equation (3.12)
s = entropy
S = interaction parameter, see equation (3.13)
T = temperature
$\mathbf{V}$ = velocity vector
α = fractional ionization
$\beta = \sqrt{(M_0^2 - 1)}$
γ = ratio of specific heats
ϵ_0 = permittivity in vacuum
λ = ion-slip parameter
μ = magnetic permeability
ρ = density
σ = electrical conductivity
ϕ = electrical potential
ϕ_B = barrier potential
ω = cyclotron frequency

Subscripts

0 = free-stream conditions
1 = first order in K
r, θ, z = components in direction of co-ordinate axis
s = stagnation conditions
T = toroidal
p = poloidal

Superscripts

* = dimensional quantities
′ (prime) = flow perturbations

Axisymmetric flow through a Helmholtz coil is the simplest experimental configuration. Perhaps its most desirable feature for this study is the distinct nature of Hall effects. In the absence of Hall effects, the induced currents are toroidal† and are given precisely by $\sigma \mathbf{V} \times \mathbf{B}$ even with non-uniform fields (so long as they are axisymmetric). The Hall effect introduces a poloidal electromotive field causing the appearance of poloidal currents and electric fields. This is in contrast to the two-dimensional rectangular geometry—the usual MHD power generator—where eddy currents always exist because of end effects, and the Hall effect modifies the existing current and electric fields rather than offering a distinct contribution (e.g. Podolsky & Sherman 1962).

Another feature of the axisymmetric geometry is that currents are not small perturbations as in many problems of linearized magnetogasdynamics (e.g. Resler & McCune 1960); Joule heating appears to first order and the flow is not isentropic. Joule heating has not received the attention it deserves as a modifier of the gas motion, with most authors pointing to the Lorentz force as the major influence on the flow. Perhaps this is because most power-generation schemes and shock-tube experiments are limited to low Mach numbers, and the effect of Joule heating in the energy equation depends quadratically on the Mach number. However, in propulsion devices where the exit Mach number is high, Joule heating may overshadow the Lorentz force in shaping the gas motion, and the axisymmetric free jet is perhaps the cleanest geometry in which these effects can be observed.

In this investigation flow perturbations and Hall potentials were measured, and the magnetogasdynamic equations were employed to explain these measurements. Nominal values of the dimensionless parameters important in the experiment are: Mach number, $M \approx 3$; Reynolds number, $Re \approx 1000$; interaction parameter, $S \approx 1$; Hall parameter, $K \approx 1$ (based on $L^* = 13{\cdot}5$ cm, a length

† Toroidal, having only an azimuthal component; poloidal, having no azimuthal component.

representing the extent of the magnetic field). With supersonic flow, compressibility effects will be important. Since the Reynolds number indicates the ratio of inertial to viscous forces, and the interaction parameter indicates the ratio of body to inertial forces, the values above imply that body and inertial forces will be comparable, and viscous forces will be negligible within the interaction region. (Viscous effects are important in the nozzle, with the boundary layer almost filling the nozzle exit.) A value of 1 for the Hall parameter implies that Hall currents can be important if the geometry of the system permits their closure. A small value for the magnetic Reynolds number indicates that induced magnetic fields will be small compared with applied magnetic fields, or that the field lines slip freely through the plasma. The problem is further characterized by the complete absence of any solid boundaries or electrodes in the system.

A number of papers have appeared describing analytical and experimental investigations of the flow of plasma and plasmoids across magnetic fields. For the most part these concern very rarefied plasmas, usually fully ionized, and the analysis is based on particle orbit theory or the Boltzmann equation (see Gilleo 1961 and Scott & Voorhies 1961), in contrast to the macroscopic treatment used here. More closely related to this study (and of great help to this author) is the work of Kemp & Petschek (1958) on the elliptical solenoid and its extension to compressible flow by Fishman *et al.* (1959) for a circular solenoid. The equations used here are identical with theirs, the analysis follows similar lines, and the major difference is in the velocity and magnetic field geometries and the boundary conditions. Ehlers (1961), Hains & Yoler (1962) and Hains, Yoler & Ehlers (1959) have studied the flow perturbations for axisymmetric channel flow assuming a scalar electrical conductivity, a problem differing from the axisymmetric free jet only in the condition at the jet boundary. More recently, Hasimoto (1964) has determined the swirl velocity induced in a free jet by Hall currents using an analysis similar to this one.

2. Experimental programme

2.1. *Apparatus and operating conditions*

The plasma tunnel consists of an arc chamber, a nozzle, and a tunnel chamber, followed by a steam ejector vacuum system. The arc burns between a $\frac{1}{5}$ in. diameter thoriated tungsten cathode and a copper-anode–nozzle assembly having a $\frac{1}{4}$ in. diameter throat. Typical running conditions are 20 V at 500 amp—a power of 10 kW with about 25 % remaining in the gas. The plasma generator and its circuitry have previously been described by Lai, Gustavson & Talbot (1958) and Brundin, Talbot & Sherman (1960), and preliminary flow studies have been reported by Brundin *et al.* (1960), Sherman & Talbot (1962), and Talbot, Katz & Brundin (1963).

The anode throat is followed by a double-cone expansion section with an exit diameter of 5·5 in. The argon is heated and ionized in the arc column, and a supersonic flow is developed in the expansion section continuing as a free jet into the tunnel chamber. The 4 ft. diameter by 8 ft. tunnel chamber has viewing ports, removable ends, side-access doors, and contains a traversing mechanism

for probe surveys of the flow; probes are positioned remotely with an accuracy of 0·010 in. Flow rates are measured with a flowmeter having a least count of 0·02 g/sec. Stagnation pressure is measured with a mercury manometer having a least count of 0·1 torr. Impact and static pressures are measured using an oil manometer having a least count of 0·001 in. oil (approximately 0·002 torr).

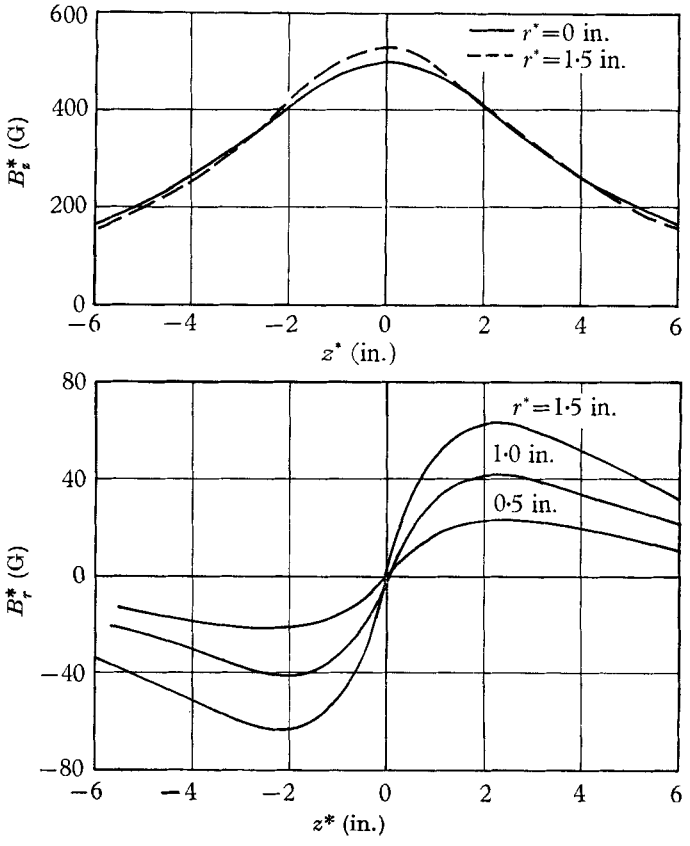

FIGURE 1. Magnetic field calibration for a coil current = 27·8 amp.

The magnetic field is supplied by Helmholtz coils having a 6 in. internal diameter, 18 in. outside diameter, and $2\frac{3}{4}$ in. thickness. Magnetic field distributions, for a single coil, are shown in figure 1 and the experimental configurations are illustrated in figure 2.

Figure 3 illustrates the Langmuir probe (hereafter called the E-probe) used in the experiments. The probe consists of three tungsten wires of 0·007 in. diameter and 5 in. length (only one is shown in the figure). The current collection area is a length of 0·140 in. on one end of the wire, the remainder being insulated with a 0·001–0·003 in. thick Al_2O_3 coating and a $\frac{1}{32}$ in. diameter ceramic tube, as shown in the sketch. The wires are supported in a rectangular brass block which is water cooled and shelters the connexions to copper lead-in wires. The probe block, cooling-water tubes, and lead-in wires are insulated with several coats of Sauereisen.

The arc chamber and arc circuit are electrically isolated from the tunnel chamber and from the Helmholtz coil. The Helmholtz coil is electrically isolated from the tunnel, and is coated with Sauereisen to prevent communication with the plasma stream. Hence, all induced currents must close within the plasma.

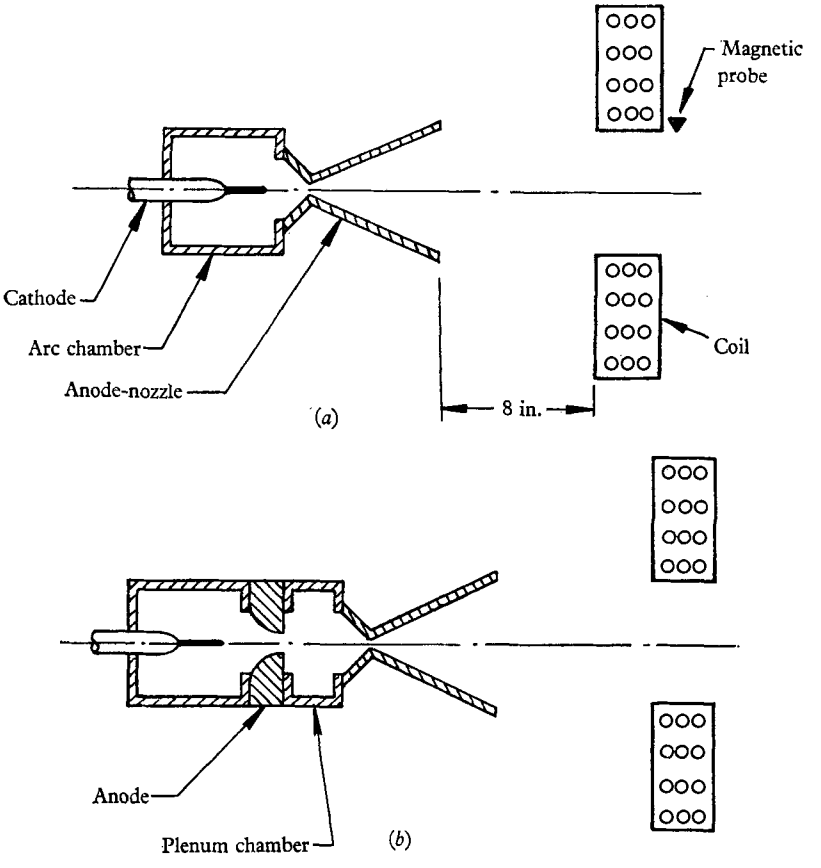

FIGURE 2(*a*) Mach 3 configuration (no plenum chamber).
(*b*) Mach 5 configuration (plenum chamber).

All Mach 3 data presented in this report were taken with the following conditions: argon flow rate, 0·58 g/sec; arc voltage, 19 V; arc current, 530 amp; stagnation pressure, 250 torr; static pressure,† 0·050 torr. For this condition, nominal values for the flow properties are: stagnation temperature, 6260 °K; total density, $0{\cdot}24 \times 10^{-4}$ kg/m^3; velocity, 2210 m/sec; ion density, 3×10^{19} ions/m^3; electrical conductivity, 500 mhos/m; magnetic Reynolds number, 0·19. Nominal values for the interaction and Hall parameters are: $S = 0{\cdot}13 \times 10^{-4}\,(B^*)^2$; $K = 0{\cdot}01\,B^*$, with B^* in gauss.

The electrical conductivity is obtained from Spitzer's result (1956) for a fully-ionized gas, and the Hall parameter is estimated from the work of Landshoff

† This is the tunnel chamber pressure and is only representative of the static pressure in the jet. The static pressure is not measurable because of excessive viscous-interaction effects on pressure probes.

(1949) in the manner described by Fishman, Lothrop, Patrick & Petschek (1959). The nominal values $T_e = 0{\cdot}3$ eV, ion saturation current = 5 mA, and $p_i^* = 0{\cdot}7$ torr, are used in the estimates. All stream properties have strong radial dependence (except T_e^* and σ^*).

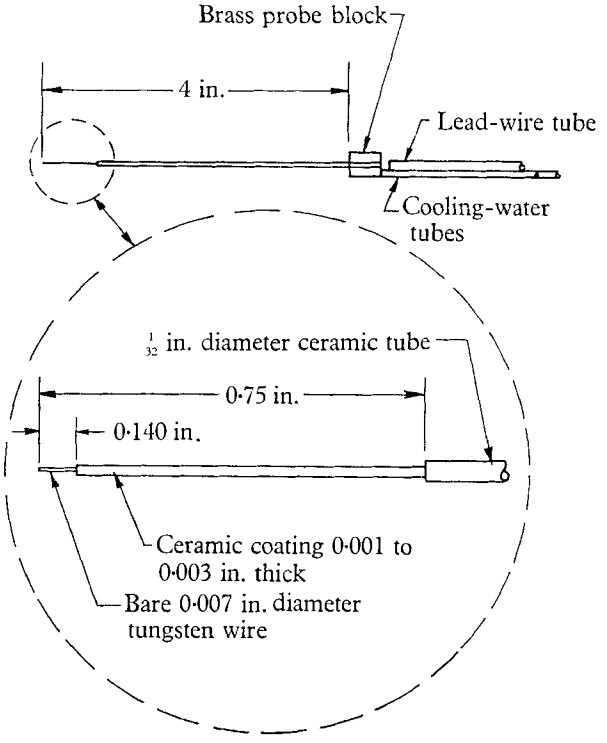

FIGURE 3. *E*-probe.

2.2. *Experiments*

Modest magnetic field strengths resulted in a pronounced disturbance of the jet as shown in figure 4 (plate 1). Flow is from the nozzle exit at the left, through the coil at the centre. An impact-pressure probe is visible downstream of the coil. The photograph shows approximately what is seen with the naked eye except that detail of the probe shock was lost in the printing process. With no magnetic field, the jet had a 3 in. diameter central core of almost constant luminosity (the 'core') surrounded by a $1\frac{1}{2}$ in. thick layer of varying luminosity (the 'outer flow'). At 1000 G, the jet was strongly channelled with a fivefold increase in core luminosity. The minimum diameter occurred near the coil centre, and the jet expanded rapidly downstream of the coil.

The magnetic field perturbation was measured with a probe located as shown in figure 2. With a reading of 250 G for the radial field component, the arc was shut off, and the meter showed no change (the minimum detectable change was 1 G). Hence, the induced magnetic field was negligible, and simple estimates confirm this observation.

Axial and radial pressure surveys (figure 6) show that the neutral atoms (which account for about 99 % of the impact pressure) participate in the flow channelling.

Apparently the collision frequency is sufficient to drag the neutrals along with the ionized components. Owing to the limited axial extent of the tunnel traverse mechanism, data were not obtained for more than 3 in. downstream of the coil centre.

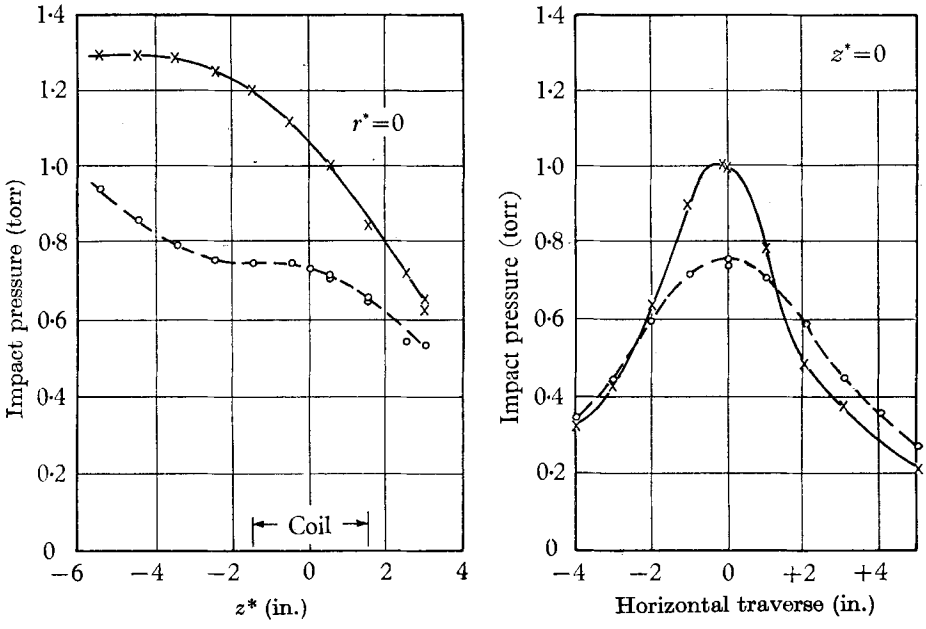

FIGURE 6. Impact Pressure Survey. —×—, coil current = 60 amp; --○--, zero coil current.

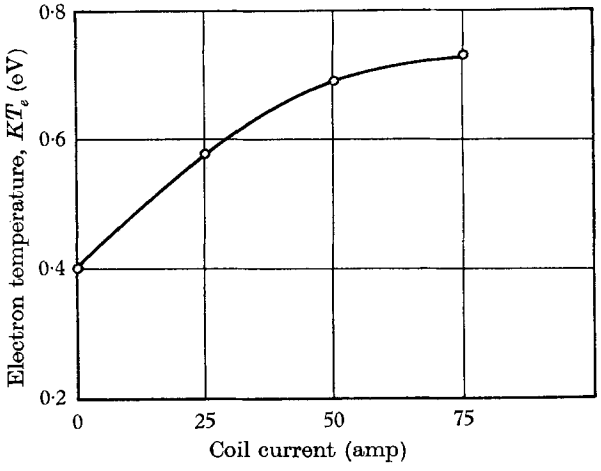

FIGURE 7. Electron temperature versus coil current for $r^* = 1{\cdot}0$ in., $z^* = 1{\cdot}5$ in.

E-probe surveys gave floating potential, saturated ion current, and electron temperature. The probe was operated near ion saturation to avoid undesirable effects such as shifts in floating potential and hysteresis. Since the electron temperature did not seem to vary significantly in the interaction region, varia-

tions in floating potential were taken as representative of variations in the plasma potential. Axial probe surveys showed that a potential was developed across the magnetic field region, which will be called the 'barrier potential', and which amounted to as much as 2 V for strong interactions. Quite by chance, it was noticed that a voltmeter connected between the nozzle and the tunnel registered a change in potential equal to the barrier potential when the magnetic field was turned on. This is reasonable since the nozzle and tunnel chamber are connected only by the plasma stream, and any induced axial potential difference should be reflected in the tunnel–nozzle potential. This allowed the barrier potential to be measured directly, and recorded as a function of magnetic field strength on an (X, Y)-plotter. Such a curve is shown in figure 8 for weak magnetic fields, and the data are in good agreement with the analysis.

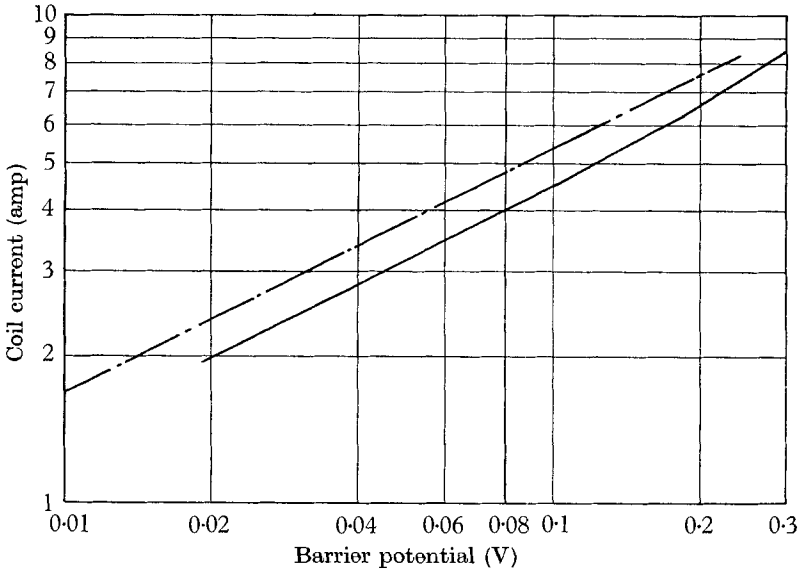

FIGURE 8. Barrier potential versus coil current; 1 amp in the coil corresponds to 18 G. —, experimental data; — · —, predicted by equation (4.18).

Electron temperatures were obtained from the Langmuir-probe data in the usual manner: (1) saturated ion current is subtracted from total probe current to yield electron current, (2) the logarithm of the electron current is plotted against the probe potential, and (3) kT_e is taken as the logarithmic decrement of the curve. This presumes the plot is a straight line. This was true for data obtained with no magnetic field, but the plots became increasingly curved with increasing magnetic field strengths. This curvature could result from probe-surface effects, or it could indicate a non-Maxwellian distribution. Electron temperatures taken at $r^* = 0$ and $z^* = 1{\cdot}5$ (figure 7) are representative of the rise in T_e that occurs throughout the magnetic interaction region. With no magnetic field, T_e ranged from 0·28 to 0·40 eV for all tests and all positions within the core. These values are lower than obtained previously by Brundin *et al.* (1960) and Sherman & Talbot (1962) using stagnation-point probes, a result consistent with the expecta-

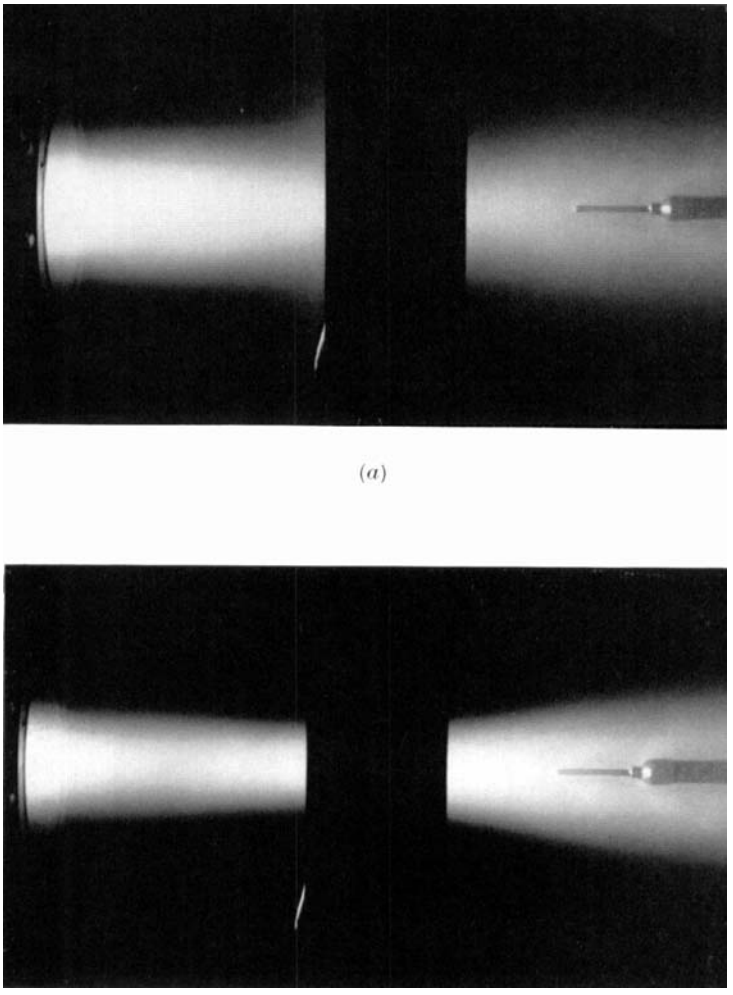

(*a*)

(*b*)

FIGURE 4. Flow photograph at Mach 3 (no plenum chamber). Photographs taken at $\frac{1}{30}$ sec, $f/11$, using Polaroid type 42 film. (*a*) Zero coil current; (*b*) 50 amp coil current.

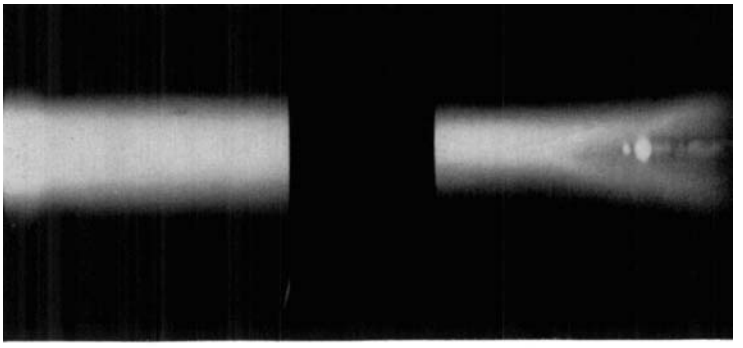

(*a*)

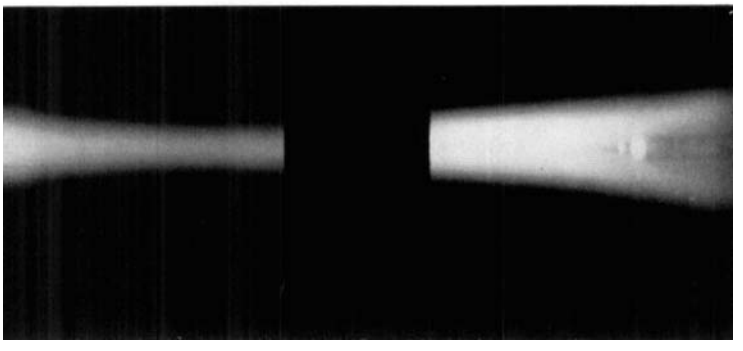

(*b*)

FIGURE 5. Flow photograph at Mach 5 (with plenum chamber). Photographs taken at $\frac{1}{30}$ sec, $f/5{\cdot}6$, using Polaroid type 42 film. (*a*) Zero coil current; (*b*) 50 amp coil current.

tion of electron heating in the bow shock on a stagnation-point probe. In some recent work in the same apparatus, Robben (1963) has estimated electron temperatures of 0·17–0·30 eV in helium based on recombination spectra, and Brundin (1964) has measured electron temperatures of 0·20–0·30 eV in argon, using Langmuir probes.

At Mach 3, the condition of all early tests, Joule heating was shown by the analysis to have a minor influence on the flow (§ 5). The analysis predicted that at high Mach numbers Joule heating would dominate in shaping the gas motion, and it would affect the flow quite differently from the body force. To confirm this finding, data were obtained at the somewhat higher Mach number of 5 (see figure 5, plate 2), and, although the increase in Mach number is slight, there is a significant change in the shape of the perturbed jet. The higher Mach number was obtained simply by introducing a plenum chamber between the anode and the nozzle (figure 2), thereby removing a heat source from the divergent nozzle section.

3. Basic equations and calculation model

The experimental flow should be described by macroscopic equations for a thermally non-conducting, inviscid, compressible gas, with a current equation which includes the Hall effect. The following equations satisfy these conditions:

$$\nabla.\rho\mathbf{V} = 0, \tag{3.1}$$

$$\rho\mathbf{V}.\nabla\mathbf{V} + (1/\gamma M_0^2)\nabla p - S\mathbf{j}\times\mathbf{B} = 0, \tag{3.2}$$

$$\mathbf{V}.\nabla s = S\gamma M_0^2(1+\alpha)j^2/p, \tag{3.3}$$

$$\nabla.\mathbf{E} = q, \tag{3.4}$$

$$\nabla\times\mathbf{E} = 0, \tag{3.5}$$

$$\nabla.\mathbf{B} = 0, \tag{3.6}$$

$$\nabla\times\mathbf{B} = R_M\mathbf{j}, \tag{3.7}$$

$$ds = \{1/(\gamma-1)\}\{dp/p - \gamma\, d\rho/\rho\}, \tag{3.8}$$

$$\sigma(\mathbf{E}+\mathbf{V}\times\mathbf{B}) = \mathbf{j} + K\mathbf{j}\times\mathbf{B} - \lambda(\mathbf{j}\times\mathbf{B})\times\mathbf{B}. \tag{3.9}$$

These were taken from the works of Kemp & Petschek (1958) and Fishman *et al.* (1959), and are discussed extensively in their work. The equations were made dimensionless using the variables

$$\left.\begin{aligned} &r = r^*/L^*, \quad z = z^*/L^*, \quad \mathbf{V} = \mathbf{V}^*/V_0^*, \quad \rho = \rho^*/\rho_0^*, \\ &p = p^*/p_0^*, \quad s = s^*/R^*, \quad \mathbf{E} = \mathbf{E}^*/V_0^*B_0^*, \\ &q = L^*q^*/\epsilon_0^*V_0^*B_0^*, \quad \mathbf{B} = \mathbf{B}^*/B_0^*, \quad \mathbf{j} = \mathbf{j}^*/\sigma^*V_0^*B_0^*, \quad \sigma = \sigma^*/\sigma_0^*, \end{aligned}\right\} \tag{3.10}$$

and the parameters defined by:

$$\text{free-stream Mach number } M_0 = (\rho_0^*V_0^{*2}/\gamma p_0^*)^{\frac{1}{2}}, \tag{3.11}$$

$$\text{magnetic Reynolds number } R_M = V_0^*L^*\sigma^*\mu^*, \tag{3.12}$$

$$\text{interaction parameter } S = \sigma_0^*L^*B_0^{*2}/\rho_0^*V_0^*, \tag{3.13}$$

$$\text{Hall parameter } K = \sigma_0^*B_0^*K^*, \tag{3.14}$$

$$\text{ion-slip parameter } \lambda = \sigma_0^*B_0^{*2}\lambda^*. \tag{3.15}$$

Here ρ_0^*, p_0^*, V_0^* and σ_0^* are evaluated in the undisturbed jet, and B_0^* is the value of the applied magnetic field at the coil centre. R_M and λ will be considered negligible.

Calculations will be based on the slug-flow model illustrated in figure 9, which has the following conditions:

$$\left.\begin{aligned} &p_0 = 1, \quad \rho_0 = 1, \quad s = 0 \quad \text{for all } r \quad \text{and as} \quad z \to -\infty, \\ &\sigma = 1 \quad \text{for} \quad r \leqslant b \quad \text{and all } z, \\ &\quad = 0 \quad \text{for} \quad r > b \quad \text{and all } z, \\ &\mathbf{V} = 1\mathbf{e}_z \quad \text{for} \quad r < a \quad \text{and} \quad z \to -\infty, \\ &\quad = 0 \quad \text{for} \quad r \geqslant a \quad \text{and} \quad z \to -\infty, \\ &B_r = rz\,e^{-z^2}, \quad B_z = e^{-z^2}. \end{aligned}\right\} \tag{3.16}$$

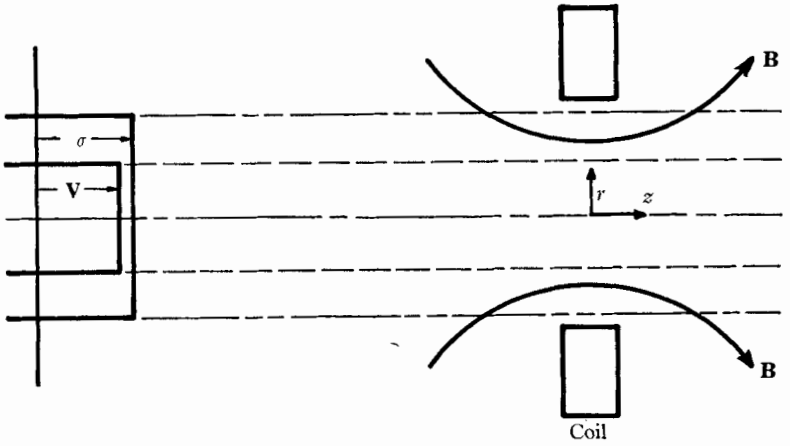

FIGURE 9. Slug-flow model.

In this model, radial distributions of velocity and electrical conductivity are treated as square waves of width $2a$ and $2b$. The magnetic field is represented by analytical expressions which only approximate the field used in the experiments. They show the same general character as the curves in figure 1, and their use presents a real advantage in obtaining closed-form solutions in §4. The expressions do satisfy $\nabla . \mathbf{B} = 0$. The characteristic length of the problem L^* is that value of z for which B_z decreases by a factor of e. In the expression assumed for B_r, its value increases linearly with r without limit. This is greatly in error when $2r$ is greater than the inside diameter of the Helmholtz coil and leads to the practical limitation $a < 0{\cdot}5$, $b < 0{\cdot}5$. This model is not essential to what follows, but it greatly simplifies the calculations.

4. Electric and current fields

The current equation is solved to zero order in S (no flow perturbations) in an attempt to describe the electric fields observed in the experiments. The solution is constructed as a power series in K with results carried to second order. This limits K to values of order unity, but the solution does shed light on the nature of

Hall effect in this geometry, and, hopefully, provides a stepping stone toward a complete solution.

It is assumed that all variables can be represented by a series of the form†

$$\mathbf{j} = \mathbf{j}_0 + \mathbf{j}_1 K + \mathbf{j}_2 K^2 + \ldots. \tag{4.1}$$

The current flowing in the absence of Hall effect j_0 is called the 'zero-order current'. The coefficient $\mathbf{j}_n$ $(n = 1, 2, 3, \ldots)$ is called the 'nth-order Hall current'. Substituting into equation (3.9) and separating terms in equal powers of K, we obtain

$$\mathbf{j}_n - \sigma \mathbf{E}_n = -\mathbf{F}_{n-1}, \tag{4.2}$$

where $\mathbf{F}_{-1} \equiv -\sigma \mathbf{V} \times \mathbf{B}$, and $\mathbf{F}_m \equiv \mathbf{j}_m \times \mathbf{B}$ $(m = 0, 1, 2, \ldots)$.

$\mathbf{F}_n$ is the Lorentz force produced by the nth-order current. The radius of convergence of this series will always be greater than $K < 1$, but no criterion has been established for its greatest lower bound.

The current to each order $\mathbf{j}_n$ is driven by an electromotive field equal to $-\mathbf{F}_{n-1}$. If $\mathbf{F}_{n-1}$ is solenoidal, the currents close without charge separation and $\mathbf{E}_n = 0$. However, if $\mathbf{F}_{n-1}$ is not solenoidal, there results a slight charge imbalance and an electric field $(\mathbf{E}_n)$ which is just sufficient to yield a solenoidal $\mathbf{j}_n$. For odd n, the electromotive field is toroidal, hence solenoidal, with the result that $\mathbf{j}_0$ is toroidal and $\mathbf{E}_0 = 0$, $\mathbf{j}_1$ and $\mathbf{E}_1$ are poloidal, $\mathbf{j}_2$ is toroidal and $\mathbf{E}_2 = 0$. This means that we need only solve for $\mathbf{E}_1$ to get the electric current to second order in K.

4.1. *Hall potentials to first order in K*

Taking the divergence of equation (4.2) (with $n = 1$),

$$\nabla^2 \phi_1 = -\nabla . \mathbf{F}_0 = -\nabla . (\sigma \mathbf{V} \times \mathbf{B}) \times \mathbf{B} \equiv -q(r, z), \tag{4.3}$$

which in cylindrical co-ordinates takes the form

$$(\phi_1)_{rr} + (1/r)(\phi_1)_r + (\phi_1)_{zz} = -q(r, z). \tag{4.4}$$

$q(r, z)$ is the first-order charge distribution, and in the slug-flow model it is antisymmetric about $z = 0$. Some care must be exercised in the treatment of $q(r, z)$ since the discontinuities in V and σ at $r = a$ and b result in a surface charge (at a or b, whichever is smaller). We consider only the case $a \leqslant b$. The boundary conditions are:

$$\left.\begin{aligned} &\phi_1 = 0 \quad \text{at} \quad z = 0, \\ &\nabla \phi_1 \to 0 \quad \text{as} \quad |r| \to \infty \quad \text{and} \quad |z| \to \infty, \\ &\mathbf{e}_r . \nabla \phi_1 = 0 \quad \text{at} \quad r = b. \end{aligned}\right\} \tag{4.5}$$

The first condition is a convenient arbitrary choice. The second condition requires that the electric field (but not the potential) vanishes at infinity. The third condition prohibits current flow across the plasma boundary. This problem is analogous to heat conduction in an infinite cylinder with distributed heat

† A similar procedure could be used to include the effect of ion slip.

sources whose boundary ($r = b$) is insulated. The solution is obtained using the finite Hankel transform† (see Sneddon 1946), defined by

$$\zeta_0\{f(r)\} = \int_0^b rf(r)\,J_0(k_i r/b)\,dr = \bar{f}(k_i). \tag{4.6}$$

The k_i are roots of the equation

$$(k_i/b)\,J_1(k_i) = 0, \tag{4.7}$$

and the inverse is

$$f(r) = \zeta_0^{-1}\{\bar{f}\} = \frac{2}{b^2}\sum_i \bar{f}(k_i)\,\frac{J_0(k_i r/b)}{\{J_0(k_i)\}^2}. \tag{4.8}$$

The transform of equation (4.4) is

$$(\bar{\phi}_1)_{zz} - (k_i/b)^2\,\bar{\phi}_1 = -\bar{q}(k_i, z), \tag{4.9}$$

and a solution satisfying the boundary conditions is

$$\bar{\phi}_1(k_0, z) = \int_0^z t\,\bar{q}(k_0, t)\,dt + z\int_z^\infty \bar{q}(k_0, t)\,dt \tag{4.10}$$

for $i = 0$ and

$$\bar{\phi}_1(k_i, z) = \frac{b}{2k_i}\int_0^\infty \left[\exp\left\{-\left|k_i\left(\frac{t-z}{b}\right)\right|\right\} - \exp\left\{-k_i\left(\frac{t+z}{b}\right)\right\}\right]\bar{q}(k_i, t)\,dt \tag{4.11}$$

for $i = 1, 2, 3, \ldots$.

Inverted by means of equation (4·8), the complete solution for ϕ_1 is

$$\phi_1(r, z) = \frac{2}{b^2}\bar{\phi}_1(k_0, z) + \sum_{i=1}^{\infty} \bar{\phi}_1(k_i, z)\,\frac{J_0(k_i r/b)}{\{J_0(k_i)\}^2}. \tag{4.12}$$

Since both $(\bar{\phi}_1)_{zz}$ and $\bar{q}(k_i, z)$ vanish at $z = 0$ and $z \to \pm\infty$, then, as shown by (4.9), $\bar{\phi}_1$ must vanish at these limits except for $k_0 = 0$. Hence, only the zero-order‡ term contributes to a net rise in potential across the interaction region, and the barrier potential is given to first order in K by

$$\phi_{1B} \equiv 2[\phi_1(\infty, r) - \phi_1(0, r)] = (2/b^2)\int_0^\infty t\,\bar{q}(k_0, t)\,dt. \tag{4.13}$$

Now these results will be applied to the slug-flow model defined in equation (3·16).

$$q = \nabla . \mathbf{F}_0 = h_1(r)\,z\exp(-2z^2) - h_2(r)\,\frac{\partial}{\partial z}\{z^2\exp(-2z^2)\}, \tag{4.14}$$

where

$$h_1(r) \equiv \frac{1}{r}\frac{\partial}{\partial r}(\sigma V r^3), \quad h_2(r) \equiv \sigma V r^2.$$

The transform of $q(r, z)$ is

$$\bar{q}(k_i, z) = \bar{h}_1(k_i)\,z\exp(-2z^2) - \bar{h}_2(k_i)\,\frac{\partial}{\partial z}\{z^2\exp(-2z^2)\}, \tag{4.15}$$

† The author is grateful to P. L. Chambré for suggesting the use of the Hankel transform.

‡ Care must be exercised to avoid confusion here. This entire section concerns only the first-order Hall potential; yet its solution is in terms of an infinite series, and the terms of this series will be referred to as zero order, first order, etc.

where by (4.6)

$$\bar{h}_1(0) = 0,$$

$$\bar{h}_2(0) = \tfrac{1}{4}a^4,$$

$$\bar{h}_1(k_i) = -a^2\{J_0(k_i a/b) - 2(b/k_i a)\,J_1(k_i a/b)\},$$

$$\bar{h}_2(k_i) = (ba^3/k_i)\,[\{1 - 4(b/k_i a)^2\}J_1(k_i a/b) + 2(b/k_i a)\,J_0(k_i a/b)] \quad (i = 1, 2, 3, \ldots).$$

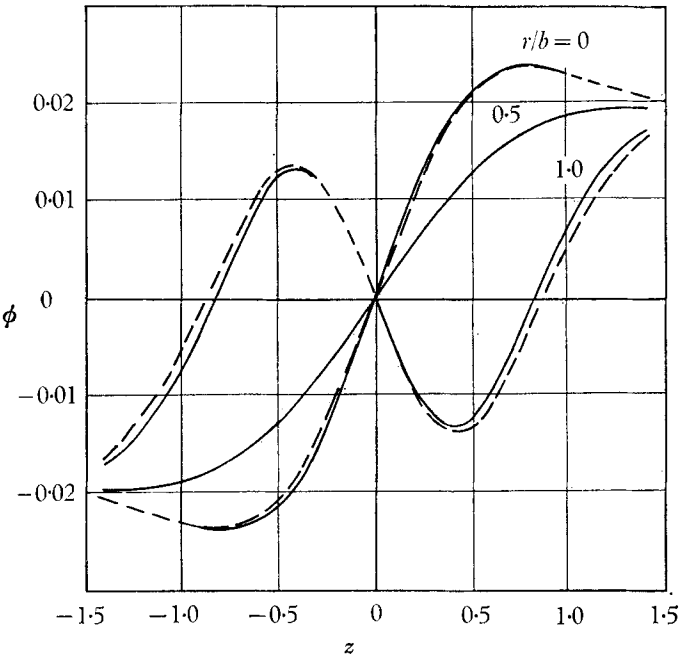

FIGURE 10. Potential to first order in K for $a = b = 0{\cdot}5$. ——, From equation (4.16); – – –, from equation (4.20).

Substituting $\bar{q}(k_i, z)$ into equations (4.10) and (4.11), and thence into equation (4.12), one finds the Hall potential to first order in K:

$$\phi_1(r,z) = \tfrac{1}{16}\sqrt{(\pi/2)}\,(a^4/b^2)\{\mathrm{erf}(\sqrt{2}z) - 2\sqrt{(2/\pi)}\,z\exp(-2z^2)\}$$
$$+ (1/b)\sum_{i=1}^{\infty}(1/k_i)\{(\bar{h}_1 - 2\bar{h}_2)Z_A + 4\bar{h}_2 Z_B\}\frac{J_0(k_i r/b)}{\{J_0(k_i)\}^2}, \quad (4.16)$$

where

$$Z_A \equiv \int_0^\infty \left[\exp\left\{-\left|k_i\left(\frac{t-z}{b}\right)\right|\right\} - \exp\left\{-k_i\left(\frac{t+z}{b}\right)\right\}\right] t\exp(-2t^2)\,dt,$$

$$Z_B \equiv \int_0^\infty \left[\exp\left\{-\left|k_i\left(\frac{t-z}{b}\right)\right|\right\} - \exp\left\{-k_i\left(\frac{t+z}{b}\right)\right\}\right] t^3\exp(-2t^2)\,dt.$$

The first eight terms of the series were evaluated for $a = b = 0{\cdot}5$, and the result is shown in figure 10.

4.2. *Barrier potential*

From equations (4.13) and (4.15), the barrier potential is

$$\phi_{1B} = \{\sqrt{(2\pi)}/16\}(a^4/b^2). \tag{4.17}$$

It is identical with that potential which would develop were the charge at each axial location z to be smeared uniformly across the disk of radius b and the problem treated as one-dimensional. In dimensional form, the barrier potential to first order in K is

$$\phi_B^* = \{\sqrt{(2\pi)}/16\} L^* V_0^* B_0^* K(a^4/b^2) + O(K^3 B^3), \tag{4.18}$$

and this expression has been compared with the measured tunnel-to-nozzle potential in figure 8, assuming an effective slug diameter of $a = b = 0{\cdot}5$. The agreement is quite good up to a coil current of 10 amp ($B_0^* \approx 180$ G, $K \approx 1{\cdot}8$, $S \approx 0{\cdot}4$), after which the data depart from B^2 dependence.

It is interesting to compare the barrier potential with the electromotive force $\mathscr{E}$ developed across the interaction region. The electromotive force is the integral of the electromotive field, i.e.

$$\mathscr{E} \equiv -\int_{-\infty}^{+\infty} \mathbf{F}_0 . \mathbf{e}_z \, dz = r^2 \int_{-\infty}^{+\infty} z^2 \exp(-2z^2)\, dz = \{\sqrt{(2\pi)}/8\} r^2. \tag{4.19}$$

Its maximum value is $\mathscr{E}_{\max} = \{\sqrt{(2\pi)}/8\} a^2$. If $a = b$, then $\phi_{1B}/\mathscr{E}_{\max} = \frac{1}{2}$; only one half of the maximum e.m.f. is developed across the interaction region. If $b > a$, then $\phi_{1B}/\mathscr{E}_{\max} = a^2/2b^2$, and in the limit of large b the barrier potential vanishes.

4.3. *Small jet approximation*

We may obtain a solution valid for small b by use of Taylor series expansions for Z_A and Z_B while retaining terms to order b^4. The infinite series of equation (4.16) then become Dini expansions (see Watson 1944) of polynomials in r with the result that†

$$\phi_1(r,z) = (b^2/16)\sqrt{(\tfrac{1}{2}\pi)}\,\mathrm{erf}(\sqrt{2}z) + [\tfrac{1}{8} - \tfrac{1}{2}(r/b)^2] b^2 z \exp(-2z^2)$$
$$+ \tfrac{1}{4}[\tfrac{2}{3} - 2(r/b)^2 + (r/b)^4] b^4 (z^2 - 1) z \exp(-2z^2) + O(b^6). \tag{4.20}$$

This equation is compared in figure 10 (broken lines) with the result obtained for $a = b = 0{\cdot}5$ from equation (4.16), and the agreement is excellent. The two curves for $r/b = 0{\cdot}5$ are indistinguishable in the figure, their values differing by less than 2 %. The expression assumed for **B** in the slug-flow model (3.16) is only good for small values of b anyway, and is probably a greater limitation on the above expression (in fact on the entire analysis) than is the neglect of terms of order b^6. Hence, this result will be used in what follows to obtain the currents to first and second order in K.

† E. V. Laitone was helpful in clarifying this point.

4.4. *Hall current to first order in K*

Equation (4.20) can be used to present a simple picture of the Hall current structure. Substituting into equation (4.2) with $n = 1$ and retaining terms to order b^3 we obtain

$$j_{1z} = b^2\{\tfrac{1}{4} - \tfrac{1}{2}(r/b)^2\}\{2z^2 - 1\}\exp(-2z^2) + O(b^4), \tag{4.21}$$

$$j_{1r} = b^3(r/b)\{1 - (r/b)^2\}\{z^2 - 1\}z\exp(-2z^2) + O(b^5). \tag{4.22}$$

A sketch of this distribution (figure 11) shows three sets of current loops each in the form of a ring vortex. Because of the factor $\exp(-2z^2)$, the centre loop carries

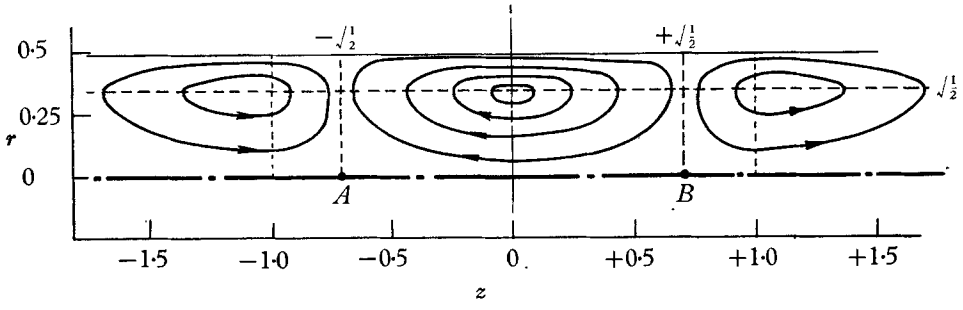

FIGURE 11. Sketch of Hall currents to first order in K.

the largest currents and is responsible for the rapid rise of potential along the axis. The outer loops carry current in the opposite direction and cause a partial cancellation of the potential rise. Points A and B represent maxima and minima of the potential on the axis. It must be remembered that this is superimposed on the zero-order currents given by $\mathbf{j} = \sigma\mathbf{V} \times \mathbf{B}$.

4.5. *Hall current to second order in K*

The second-order currents are given by equation (4.2) with $n = 2$:

$$\mathbf{j}_2 = -\mathbf{j}_1 \times \mathbf{B} \quad (\mathbf{E}_2 = 0).$$

Using the approximate expressions for $\mathbf{j}_1$ obtained for small b (4.21) and (4.22), the second-order current is

$$\mathbf{j}_2 = b^3(r/b)\,z\exp(-3z^2)\{\tfrac{1}{2}z^2 + \tfrac{1}{2}(r/b)^2 - \tfrac{3}{4}\}\,\mathbf{e}_\theta + O(b^5),$$

and the total toroidal current is

$$\mathbf{j}_T = rz\,e^{-z^2}[1 + K^2b^2\exp(-2z^2)\{\tfrac{1}{2}z^2 + \tfrac{1}{2}(r/b)^2 - \tfrac{3}{4}\}]\,\mathbf{e}_\theta + O(K^4, b^5). \tag{4.23}$$

5. Flow perturbations

To explain the observed flow perturbations, characteristics calculations are made using the linearized equations and the slug-flow model (with $b \geqslant a$). Only the zero-order currents ($\mathbf{j} = \sigma\mathbf{V}_0 \times \mathbf{B}$) are considered in the calculation. This

rather simple model proves quite successful in displaying the features observed in the experiments. The equations are linearized by introducing

$$\left.\begin{aligned} \mathbf{V} &= \mathbf{V}_0 + S\mathbf{V}', \quad \rho = 1 + S\rho', \\ p &= 1 + Sp', \qquad s = 0 + Ss', \end{aligned}\right\} \tag{5.1}$$

with the result that

$$\frac{\partial}{\partial z}\rho' + \nabla . \mathbf{V}' = 0, \tag{5.2}$$

$$\mathbf{e}_z . \nabla \mathbf{V}' + (1/\gamma M_0^2)\nabla p' = \mathbf{j} \times \mathbf{B}, \tag{5.3}$$

$$\mathbf{e}_z . \nabla s' = \gamma M_0^2 (1+\alpha) j^2, \tag{5.4}$$

$$p' = \gamma\rho' + (\gamma - 1)\, s', \tag{5.5}$$

for $r \leqslant a$, and where $\mathbf{j} = \mathbf{e}_z \times \mathbf{B}$. The Joule heating ($j^2$) term is multiplied by M_0^2 in the perturbation equations implying its dominance at high Mach numbers, and the calculations confirm this.

These equations can be integrated along their characteristics which are defined by (see Courant 1962):

$$\left.\begin{aligned} r &= \text{const. (twice)}, \\ r + (1/\beta) z &= \eta, \\ r - (1/\beta) z &= \zeta, \end{aligned}\right\} \tag{5.6}$$

where $\beta^2 = M_0^2 - 1$. The first two characteristics correspond to the integration with respect to z of equations (5.3) (z-component) and (5.4),

$$V_z' + (1/\gamma M_0^2)\, p' = -\int_{-\infty}^{z} B_r^2 \, d\zeta, \tag{5.7}$$

$$s' = \gamma M_0^2 (1+\alpha) \int_{-\infty}^{z} B_r^2 \, d\zeta, \tag{5.8}$$

and for the slug-flow model

$$\int_{-\infty}^{z} B_r^2 \, d\zeta = \tfrac{1}{8}\sqrt{(\tfrac{1}{2}\pi)}\{1 + \operatorname{erf}(\sqrt{2}z)\} - \tfrac{1}{4} z \exp(-2z^2). \tag{5.9}$$

By making suitable linear combinations of equations (5.2)–(5.5) (when written in cylindrical co-ordinates) one can obtain two additional equations which are integrable along the characteristics η and ζ,

$$2\frac{\partial}{\partial \zeta}(p'/\gamma M_0^2 - V_r'/\beta) = C_1 - C_2, \tag{5.10}$$

$$2\frac{\partial}{\partial \eta}(p'/\gamma M_0^2 + V_r'/\beta) = C_1 + C_2, \tag{5.11}$$

where

$$\left.\begin{aligned} C_1 &= (\mathbf{j} \times \mathbf{B}) . \mathbf{e}_r = B_r B_z, \\ C_2 &= (\mathbf{j} \times \mathbf{B}) . \mathbf{e}_r + M_0^2(\gamma - 1)(1+\alpha) j^2 - V_r/r, \\ &= B_r^2 + M_0^2(\gamma - 1)(1+\alpha) B_r^2 - V_r/r. \end{aligned}\right\} \tag{5.12}$$

Note that C_1 and C_2 are functions of r and z, and C_2 involves the unknown quantity V_r/r.

5.1. *Numerical solution for a slug-flow model*

Equations (5.10) and (5.11) cannot be integrated in closed form because V_r/r appears in C_2. The solution is obtained by making a step-by-step calculation from left to right through a characteristic net. The methods are conventional, but several points should be mentioned:

(1) In proceeding from net point A to net point B, C_1 and C_2 are evaluated at net point A.

(2) The Mach net is based on M_0; it does not depend on the calculated perturbations.

(3) The free jet boundary condition is imposed by requiring that $p' = 0$ at $r = a$. In the calculation, the jet boundary is considered to always be at $r = a$, but the calculated values of V_r' are not zero there. The first-order perturbation of the boundary (or any other streamline) is found by integrating V_r' with respect to z.

(4) The mesh sizes used in the calculations are given in table 1.

M_0	Δ_r	Δ_z
3·16	0·05	0·15
6·08	0·05	0·30
10·05	0·025	0·25

TABLE 1

Calculations are for $a = 0{\cdot}5$, $\gamma = \frac{5}{3}$, $\alpha \simeq 0$ and $M_0 = 3{\cdot}16$, $6{\cdot}08$ and $10{\cdot}05$.† The results (figures 12 to 16) give p' and V_r', and with equations (5.7) and (5.8) all perturbation values can be determined.

5.2. *Discussion of flow perturbations*

All perturbations arise from electromagnetic effects through the body-force ($\mathbf{F} = \mathbf{j} \times \mathbf{B}$) and Joule-heating ($Q = j^2/\sigma$) terms in the equations of motion. Since there are no physical boundaries nor external electric circuits which extract energy from the jet, the flow is adiabatic, and the energy supplied to the fluid by Joule heating is exacted from the fluid by the body force, i.e. $\mathbf{F}.\mathbf{V} = -Q$. It is the component of $\mathbf{F}$ parallel to $\mathbf{V}$ (F_z in this problem) that contributes to an irreversible exchange of directed and thermal energies. Hence the axial body force and Joule heating are related, and their effect on a characteristics calculation is confined to the function C_2. In a one-dimensional analysis of a free jet (see Shapiro 1953 and use the condition $dp = 0$) their net effect is to decrease velocity, density and Mach number, and to increase temperature and jet diameter.

There still remains the radial component of the body force F_r. It does no work on the flow (to first order) and results in no entropy production; it produces flow perturbations that constitute a reversible conversion of directed to thermal

† A referee commented on the limited value of a linearized analysis at Mach 10, a valid criticism in view of the magnitude of p' in figure 14. Since the actual perturbation in pressure is Sp', this limits S to rather small values for the Mach 10 calculation.

energy. The action of F_r is like that of a boundary which channels the flow, yet does no work on the fluid. In the problem under consideration, its effect is to channel the flow toward the axis for $z < 0$ and away from the axis for $z > 0$. Its effect on the characteristics calculation is confined to the function C_1.

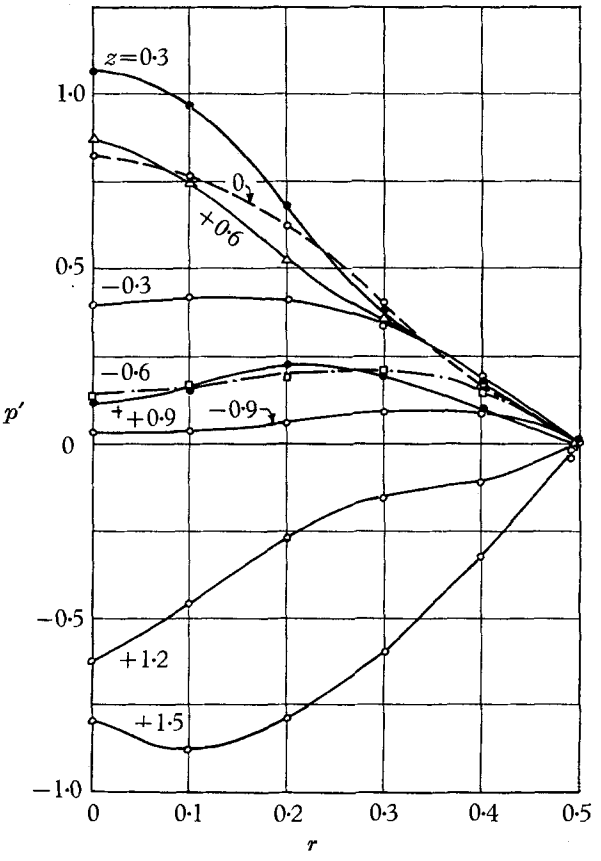

FIGURE 12. Pressure perturbation, Mach 3·16, $a = 0{\cdot}5$, $\gamma = \frac{5}{3}$.

Turning now to the calculations, the most notable result is the striking contrast between high and low Mach numbers (see p and V_r curves, figures 12, 13, 14, 15). This can be traced directly to the relative magnitudes of C_1 and C_2. For the Mach 3·16 calculation, the entire jet is channelled toward the axis with rising pressure for $z < 0{\cdot}15$. Irreversible phenomena play a minor role. The channelling is primarily due to the radial body force, and the pressure is perturbed as a consequence of the resulting radial motion.

For the Mach 10·05 calculation the flow is split; that is, the core of the jet is channelled towards the axis while the outer portion of the jet is channelled away from the axis (see V_r' curve, figure 15). In this case the irreversible phenomena paly a dominant role. Joule heating, which is proportional to r^2 and hence maximum at the edge of the jet, raises the pressure of the gas, forming a pressure 'hill'. The flow splits, moving away from the hill radially in both directions to relieve the pressure. Upstream of the coil centre, the radial body force points

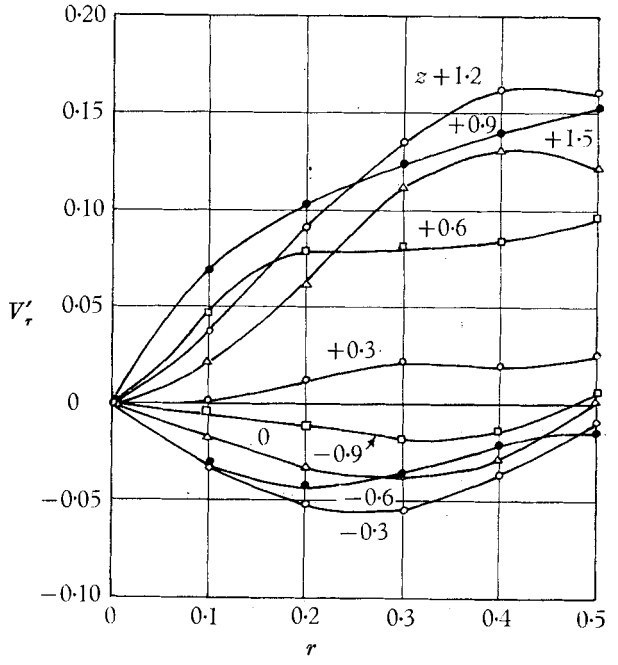

FIGURE 13. Radial velocity, Mach 3·16, $a = 0{\cdot}5$, $\gamma = \frac{5}{3}$.

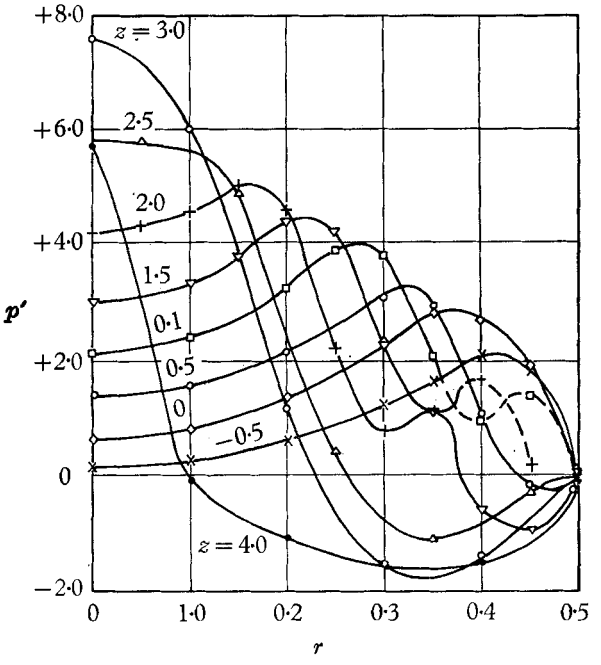

FIGURE 14. Pressure perturbation, Mach 10·05, $a = 0{\cdot}5$, $\gamma = \frac{5}{3}$.

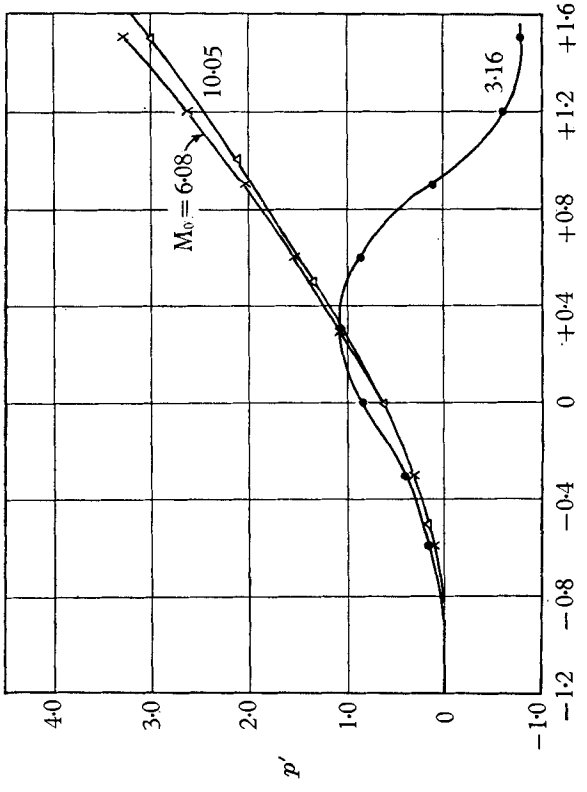

FIGURE 16. Perturbation pressure on the jet axis, $a = 0{\cdot}5$, $\gamma = \frac{5}{3}$, $r = 0$.

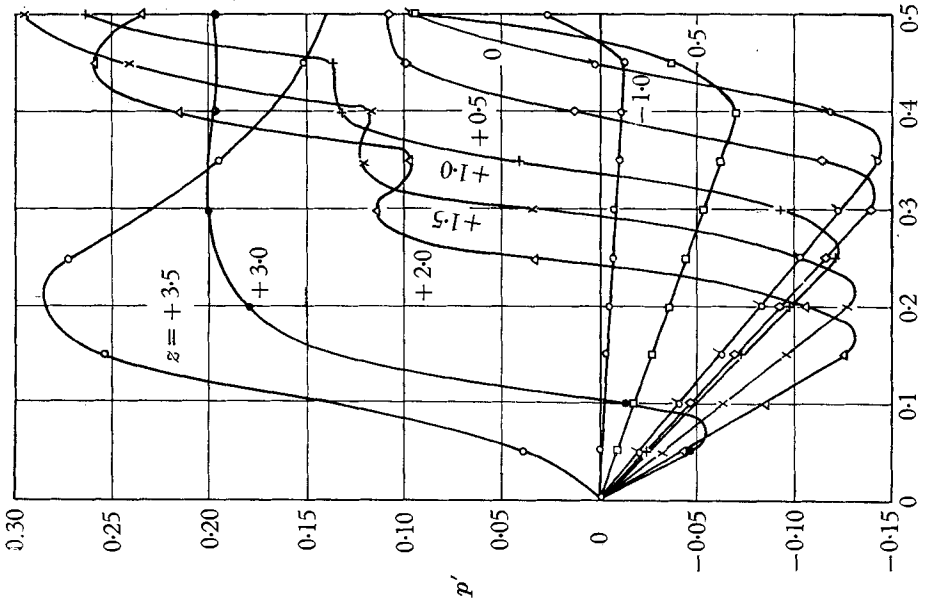

FIGURE 15. Radial velocity, Mach 10·05, $a = 0{\cdot}5$, $\gamma = \frac{5}{3}$.

towards the axis and aids in compressing the core of the jet. Its action causes the flow to 'split' to the right of the pressure-hill peak (rather than at the peak). Downstream of the coil centre, a second pressure hill is generated by the currents induced at exit from the interaction region. It is not nearly so large as the first, for here the flow is experiencing rapid expansion.

The calculations were terminated at $z < 3{\cdot}5$. Had they been continued, the jet would expand and contract in an oscillatory fashion, producing a flow structure similar to Mach diamonds. This was never observed in the experiments because of the overriding influence of viscosity for $z > 3$.

The almost perfect linearity of V_r with r for the core of the jet in the Mach 10·05 calculation occurs because both F_r and $\partial p'/\partial r$ are linear in r. By equation (5.3), $\partial V_r/\partial z$ and its integral are both linear in r.

Figure 16 shows the axial distribution of the perturbation pressure for the three Mach numbers. The initial part of the curve is almost independent of Mach number, but the maximum amplitude of the perturbation and the wavelength of the cyclical behaviour is strongly Mach-number dependent. Of special interest is the value of z for which p' changes sign; this is strongly Mach-number dependent and may serve as a convenient measure of Mach number. But, as mentioned above, viscous effects could seriously limit such an application.

6. Conclusion

The Langmuir-probe surveys showed axial and radial electric fields to be present in the interaction region with a net rise in potential which is called the barrier potential. These fields are distinctly Hall effects, and a solution to first order in K based on a slug-flow model yields closed form solutions for the Hall-potential distribution (equations (4.16) and (4.20)). Because the slug-flow model is only representative of the experimental flow, and because the flow properties are not accurately known, quantitative comparisons are not made between the analytical and experimental potential distributions. Also, all such data were recorded with strong interaction (large flow perturbations), hence fall outside the range of the first-order analysis.

Barrier potential, however, could be obtained with low values of the magnetic field by observing changes in the tunnel-to-nozzle potential, and these have been compared with good agreement with the analytical result (equation (4.18)) in figure 8. The departure of the data from the B^2 dependence predicted to first order in K is due to a combination of at least three factors: the higher-order terms in K become important and the jet velocity and diameter are changed by the interaction. All of these are of order B^4 and contribute to the deviation in the same direction.

Currents are obtained to second order in K for small values of b (equations (4.21), (4.22), (4.23)).

The first observations of the jet were obtained at Mach 3 (no plenum chamber), and are in qualitative agreement with the Mach 3·16 calculation. At higher Mach numbers, however, the calculations reveal that Joule heating becomes the major modifier of the flow, resulting in a phenomenon termed 'flow splitting'. The test Mach number was increased to about 5 (by installing a plenum chamber). This

is still rather low, yet the Mach 5 flow (figure 5, plate 2) clearly has a different shape from that of the Mach 3 flow. The minimum cross-section is upstream of the coil, and the flow appears to expand throughout most of the interaction. Figure 5 does not really show 'flow splitting' in quite the way that one would expect from the calculations; nevertheless, the outer flow does expand upstream of the coil even though the body force points towards the axis, and this is believed to be due to Joule heating.

The author is grateful to P. L. Chambré, W. Kunkel, C. L. Brundin, and to the students and staff of the Aeronautical Sciences Laboratory for their many contributions. The author is indebted to F. S. Sherman and L. Talbot for their patience in supporting and guiding this work, and for the atmosphere of inquiry that they did inspire. The work was supported by the U.S. Air Force Office of Scientific Research under contract AF 49(638)-502 and the Office of Naval Research under Contract Nonr-222(45). A more complete description has been given by Otis (1963).

REFERENCES

BRUNDIN, C. L. 1964 The application of Langmuir probe techniques to flowing ionized gases. *Univ. Calif. Aero. Sci. Div. Tech. Rep.* no. AS-64-9.

BRUNDIN, C. L., TALBOT, L. & SHERMAN, F. S. 1960 Flow studies in an arc heated low density supersonic wind tunnel. *Univ. of Calif. Eng. Proj. Rep.* no. HE-150-181.

COURANT, R. 1962 *Methods of Mathematical Physics*, vol. II, *Partial Differential Equations*, ch. 5. New York: Interscience.

EHLERS, F. E. 1961 Linearized magnetogasdynamic channel flow with axial symmetry. *ARS J.* **31**, 334–42.

FISHMAN, F., LOTHROP, J. W., PATRICK, R. M. & PETSCHEK, H. E. 1959 Supersonic two-dimensional magnetohydrodynamic flow. *The Magnetohydrodynamics of Conducting Fluids*, ed. D. Bershader, p. 120. Stanford University Press.

GILLEO, M. A. 1961 Flow of low-density high-speed plasma through a magnetic barrier. *Phys. Fluids*, **4**, 1399–1406.

HAINS, F. D. & YOLER, Y. A. 1962 Axisymmetric magnetohydrodynamic channel flow. *J. Aero. Sci.* **29**, 143–50.

HAINS, F. D., YOLER, Y. A. & EHLERS, E. E. 1959 Axi-symmetric hydromagnetic channel flow. *Boeing Res. Lab. Rep.* no. DI-82-0025. Presented at ARS Northwestern Gas Dynamics Symposium, Northwestern Univ., 24–26 August.

HASIMOTO, H. 1964 Swirl of a conducting gas due to the Hall effect. *J. Phys. Soc. Japan*, **19**, 1457–63.

KEMP, N. H. & PETSCHEK, H. E. 1958 Two-dimensional incompressible magneto-hydrodynamic flow across an elliptical solenoid. *J. Fluid Mech.* **4**, 553–84.

LAI, W., GUSTAVSON, J. & TALBOT, L. 1958 Design considerations and initial evaluation of Model B plasma generator. *Univ. of Calif. Eng. Proj. Rep.* no. HE-150-161.

LANDSHOFF, R. 1949 Transport phenomena in a completely ionized gas in presence of a magnetic field. *Phys. Rev.* **76**, 904–9.

OTIS, D. R. 1963 Computation and measurement of Hall potentials and flow-field perturbations in magnetogasdynamic flow of an axisymmetric free jet. Ph.D. thesis, University of California.

PODOLSKY, B. & SHERMAN, A. 1962 Influence of tensor conductivity on end currents in crossed field MHD channels with skewed electrodes. *J. Appl. Phys.* **33**, 1414–18.

RESLER, E. L. & MCCUNE, J. E. 1960 Some exact solutions in linearized magnetoaero-dynamics for arbitrary magnetic Reynolds number. *Rev. Mod. Phys.* **32**, 848–54.

SHERMAN, F. S. & TALBOT, L. 1962 Diagnostic studies of a low-density arc-heated wind tunnel stream. In *Hypersonic Flow Research*, ed. F. R. Riddell, vol. 7, p. 581. New York: Academic Press.

SNEDDON, I. N. 1946 Finite Hankel transforms. *Phil. Mag.* **37**, 17–25.

SPITZER, L. 1956 *Physics of Fully Ionized Gases*, chs. 2 and 5. New York: Interscience.

TALBOT, L., KATZ, J. E. & BRUNDIN, C. L. 1963 Comparison between Langmuir probe and microwave electron density measurements in an arc-heated low-density wind tunnel. *Phys. Fluids*, **6**, 559–65.

WATSON, G. N. 1944 *A Treatise on the Theory of Bessel Functions*, 2nd edition, ch. 18. Cambridge University Press.

ROBBEN, F. A. 1963 A spectrographic study of recombination in a helium plasma. *Univ. of Calif. Eng. Proj. Rep.* no. HE-150-211.

SCOTT, F. R. & VOORHIES, H. G. 1961 Plasma injection into a magnetic field. *Phys. Fluids*, **4**, 600–6.

SHAPIRO, A. H. 1953 *The Dynamics and Thermodynamics of Compressible Fluid Flow*, vol. I, ch. 8. New York: The Ronald Press Co.